Journal of Power Sources 213 (2012) 93–99

Contents lists available at SciVerse ScienceDirect

Journal of Power Sources

journal homepage: www.elsevier.com/locate/jpowsour

Short communication

Novel functionally graded acicular electrode for solid oxide cells fabricated by the freeze-tape-casting process

Yu Chen, Jacob Bunch, Tingshuai Li, Zhengping Mao, Fanglin Chen*

Department of Mechanical Engineering, University of South Carolina, 300 Main Street, Columbia, SC 29208, USA

ARTICLE INFO

Article history:
Received 2 January 2012
Received in revised form
28 March 2012
Accepted 30 March 2012
Available online 16 April 2012

Keywords:
Electrode supported solid oxide cells
Freeze-tape-casting
Acicular pore
Polarization resistance

ABSTRACT

The performance of electrode supported solid oxide cells is often limited by gas transport in the thick electrode support. In this study, a novel functionally graded acicular hydrogen electrode microstructure has been fabricated by the freeze-tape-casting method. The effects of freeze-tape-casting processing parameters such as solid loading, freezing bed temperature and tape pulling rate on the morphology of the hydrogen electrode support have been investigated. The electrochemical performance of the cells having the novel functionally graded acicular hydrogen electrode has been significantly improved. In the fuel cell mode, a high power output of 1.28 W cm^{-2} and a low polarization resistance of 0.166 Ω cm^2 have been achieved at 800 °C with H_2 as fuel and ambient air as oxidant using nickel–yttria-stabilized zirconia (YSZ) as the hydrogen electrode, YSZ as the electrolyte, and $(La_{0.75}Sr_{0.25})_{0.95}MnO_3$–YSZ as the oxygen electrode. In the electrolysis mode, a high current density of 2.3 A cm^{-2} with 30 vol% absolute humidity in the hydrogen electrode at 800 °C has been achieved with an applied cell voltage of 1.6 V. It has been revealed that the novel acicular hydrogen electrode decreases the gas diffusion resistance, thus enhancing the cell performance.

© 2012 Elsevier B.V. All rights reserved.

1. Introduction

Solid oxide cells (SOCs) have attracted a great attention as one of most promising technologies since they can be operated efficiently in fuel cell mode (solid oxide fuel cells, SOFCs) and electrolysis mode (solid oxide electrolysis cells, SOECs). Currently, there are two basic designs for SOFC and SOEC development: electrolyte supported and electrode supported solid oxide cells [1]. In electrolyte (typically yttria stabilized zirconia, YSZ) supported cells, the electrolyte's ohmic resistance limits the overall cell performance due to the thickness of electrolyte, which is typically more than 100 μm, and thus such cells usually are only suitable for operation at high temperature such as 1000 °C. In electrode supported cells, the electrolyte thickness can be decreased to 10–20 μm, significantly decreasing the cell ohmic resistance [2,3]. Therefore, electrode supported cells are more suitable for operation at intermediate or low temperature applications. Nickel based composite hydrogen electrode (Ni–YSZ) has been the most developed electrode for electrode supported solid oxide cells since it provides excellent thermal and electrical conductivity, high strength and high electrochemical catalytic capability. Further, composite hydrogen electrode can also extend the length of triple phase boundary (TPB). However, the polarization resistance, especially concentration polarization may rise significantly resulting from the resistance to mass transport through thick electrode. In addition, insufficient removal of water steam during high temperature operation both in SOFC and SOEC modes can also result in Ni oxidation and agglomeration [4].

It is widely reported that the electrode structure can be modified to minimize both activation and concentration polarization [5–7]. Suzuki et al. [5] have reported a power density of greater than 1 W cm^{-2} at 600 °C with a conventional but highly porous nickel cermet anode supported SOFC by controlling the microstructure of the anode. Providing sufficient porosity of the anode leads to significant improvement of the cell performance. Othman et al. [6] have also reported a high-performance micro tubular SOFC, which demonstrates a power density of up to 2.32 W cm^{-2} at 600 °C, achieved by increasing the effective anode porosity through adjustment of co-extrusion parameters. The presence of fingerlike structure in the asymmetric anode layer significantly improves the gas diffusion by functioning as a set of hundreds of micro-channels in the anode, subsequently enhancing the cell performance. It can be concluded that both porosity and microstructure play important roles in dictating the cell performance.

Freeze-tape-casting, which combines tape-casting and freeze-casting process to form and control complex pore structure, has been applied in the field of manufacturing catalyst support

* Corresponding author. Tel.: +1 803 777 4875; fax: +1 803 777 0106.
E-mail address: chenfa@cec.sc.edu (F. Chen).

0378-7753/$ – see front matter © 2012 Elsevier B.V. All rights reserved.
doi:10.1016/j.jpowsour.2012.03.109

structures, solid oxide fuel cells and filtration membranes [8–10]. Continuously graded pores and long-range alignment of acicular pores (<5–100 μm), which are very helpful for gas delivery in electrode, can be obtained through freeze-tape-casting process. However, freeze-tape-casting typically creates macro pores in both the bottom and the top of surfaces of the electrode substrates, dramatically increasing the difficulty in obtaining a large area defect-free dense thin electrolyte film. Introduction of a thin electrode functional layer has been shown to be an effective method to overcome this limitation and improve the adhesion between electrode and electrolyte [11,12]. In addition, the length of triple phase boundary (TPB) can be extended, where electronic phase, ionic phase and gas meet together, thus resulting in more effective electrochemical reaction sites. The NASA Glenn Research Center has developed a novel cell design and freeze-tape-casting technique to produce solid oxide fuel cells predicted to exceed a specific power density of 1.0 kW kg^{-1} [9,13]. Their bi-electrode supported cells are symmetrically prepared by taking two green parts cut from the same freeze-tape-casted YSZ scaffold, depositing a thin electrolyte layer between the tapes, laminating the tapes together, and forming the YSZ tri-layer. Ni nitrates for the hydrogen electrode and stoichiometric solution of Sr-doped $LaFeO_3$ for air electrode can be infiltrated into the YSZ scaffold. The symmetric design balanced mechanical stress and improved strength upon thermal cycling. One major concern with this design is the use of the wet infiltration technique for the electrode fabrication. Fine metallic Ni particles are susceptible to coarsening at high cell operating temperatures, leading to loss of electrical connectivity as well as reduction in the TPB sites in the hydrogen electrode, consequently resulting in potential fast cell performance degradation.

Here, we report high-performance asymmetric solid oxide cells with the hydrogen electrode supported prepared by freeze-tape-casting using the conventional Ni-YSZ cell material. The effects of solid loading, freezing bed temperature and casting tape pulling rate on the morphology of the hydrogen electrode substrate have been investigated. The button cells fabricated in this work consist of NiO–YSZ (mass ratio = 6:4) for the hydrogen electrode support and the functional layer, YSZ for the electrolyte and $(La_{0.75}Sr_{0.25})_{0.95}MnO_3$ (LSM)–YSZ for the oxygen electrode. All materials used are commercially available. The microstructure features, pore size and size distributions and electrochemical performance of cells in both fuel cell as well as electrolysis modes have been systematically evaluated.

2. Experimental

2.1. Fabrication of substrates and single cells

NiO (Sigma–Aldrich, USA) and YSZ (8YSZ, Tosoh Company, Japan) powders were purchased in this study. Water based NiO–YSZ slurry was prepared with an ammonium polyacrylate dispersant (Darvan C-N, R.T. Vanderbilt Co., Inc., Norwalk, CT), a thickener (Vanzan, R.T. Vanderbilt Co., Inc., Norwalk, CT), and an acrylic latex emulsion binder system (Duramax HA-12, Rohm & Haas, Philadelphia, PA). The freeze-tape-casting apparatus is similar to the one reported in Sofie's publication [8]. After frozen

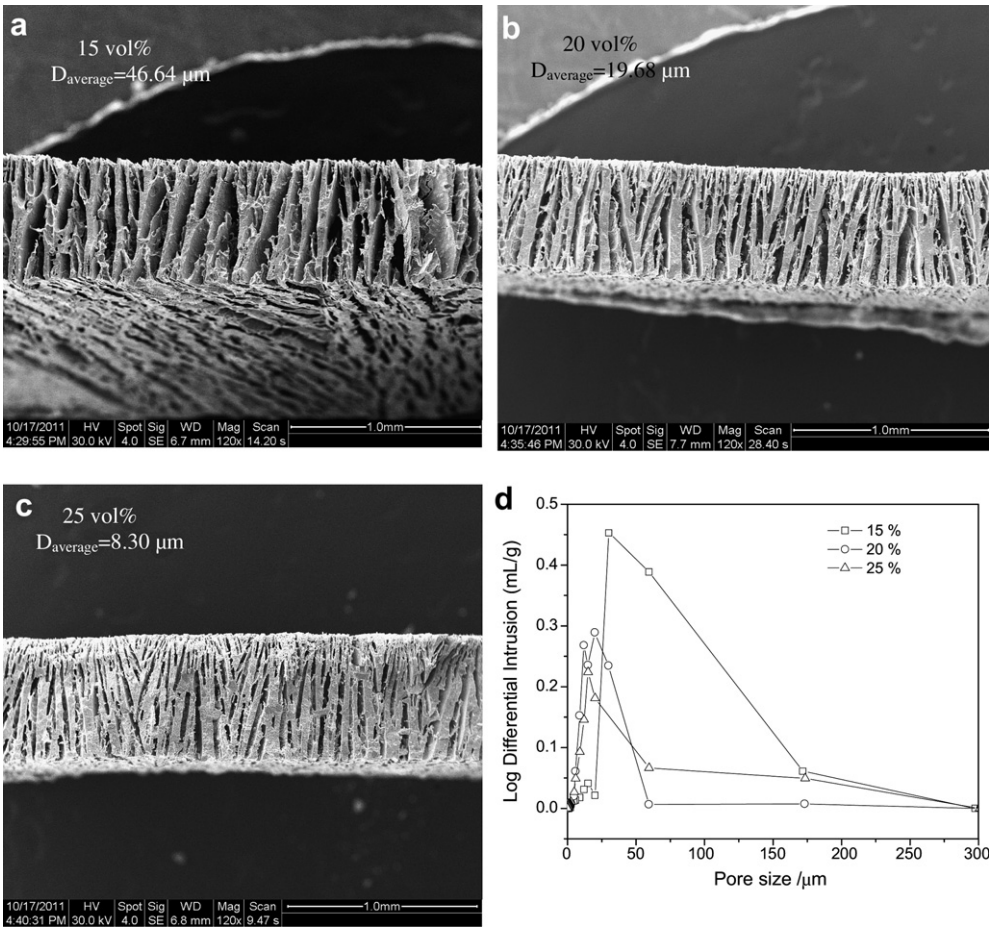

Fig. 1. Cross-section SEM images of Ni–YSZ substrates with solid loading of: (a) 15 vol%, (b) 20 vol% and (c) 25 vol%; and (d) pore size distribution for substrate with different solid loading.

about 30 min, the NiO–YSZ substrate was punched into pellets with diameter of about 19 mm. The pellets were frozen in a vacuum freeze dryer at −30 °C under 18 mtor vacuum for 12 h. The pellets were first pre-sintered at a constant heating rate of 1 °C min^{-1} to 600 °C and then at 2 °C min^{-1} to 1100 °C. A NiO–YSZ functional layer was prepared on one surface of the pre-sintered NiO–YSZ substrate by an air-brushing method and then fired at 800 °C for 2 h. The YSZ electrolyte film was prepared on the NiO–YSZ functional layer by a dip-coating method. The NiO–YSZ substrate with functional layer and electrolyte layer was then co-sintered at 1400 °C for 5 h. The LSM–YSZ composite oxygen electrode with an effective area of 0.33 cm^2 was prepared on the YSZ electrolyte surface by a screen-printing method and then sintered at 1100 °C for 2 h. For comparison, anode supported cells with the same electrolyte and cathode materials have also been prepared by dry-pressing, dip-coating and screen-printing method. For the microstructure study, the NiO–YSZ substrates without YSZ film were prepared by sintering the green substrates at 1400 °C for 5 h and then reduced at 800 °C for 12 h in hydrogen.

2.2. Characterization

The microstructure of the Ni–YSZ hydrogen electrode substrate was characterized using a scanning electron microscope (SEM, FEI Quanta 200). Pore size, pore size distribution and porosity of the Ni–YSZ substrate were determined by a mercury intrusion method (Micromeritics AutoPore IV 9500). The current density–voltage curves as well as the impedance spectra of the solid oxide cells were measured with a four probe method using a multi-channel Versa STAT (Princeton Applied Research) at the operating temperature range from 700 °C to 800 °C. The cell electrochemical performance testing system can be seen in our previous work [14]. In the SOFC test, humidified hydrogen (3% H_2O/97% H_2) was used as fuel while ambient air was used as oxidant. In the SOEC test, the amount of water vapor in the gas mixture in the hydrogen electrode was continuously measured in terms of absolute humidity (AH, the vol% of humidity in the total gas volume) using an on-line humidity sensor (Vaisala Model HMP 337). Hydrogen flow rate was controlled at 40 sccm by a mass flow controller (APEX, Alicat Scientific). The cell polarization resistance (R_p) was determined from the difference between the low and high frequency intercepts of the impedance spectra with the real axis in the Nyquist plot.

3. Results and discussion

3.1. Novel microstructure of Ni–YSZ prepared by freeze-tape-casting

In the aqueous freeze-tape-cast process, micron-sized ice crystals start to form in the casted tape at the Mylar side (lower temperature region) and then grow larger and larger towards the top of the tape. A natural gradient in porosity can be formed after the ice crystals have been removed by sublimation in a freeze dryer under vacuum. Therefore, it is necessary to investigate how the processing parameters such as solid loading, freezing bed

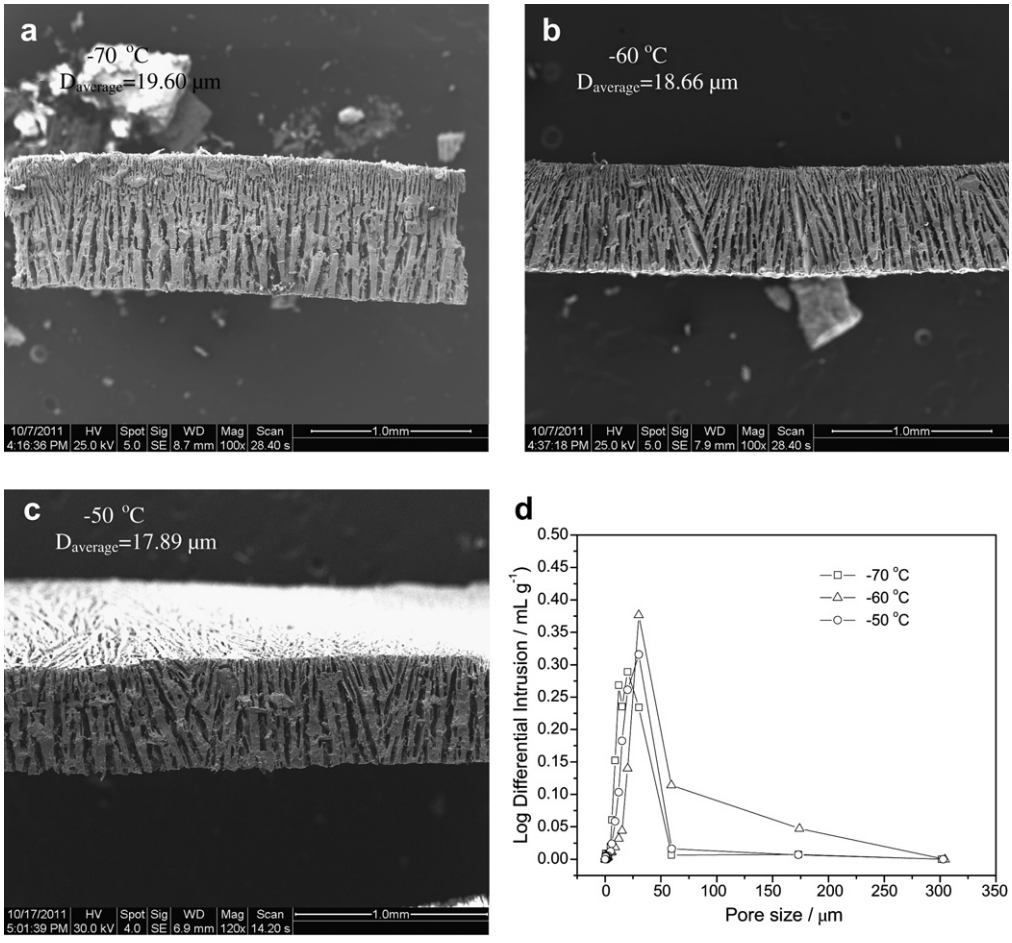

Fig. 2. Cross-section SEM images for Ni–YSZ substrates frozen at (a) −70 °C, (b) −60 °C and (c) −50 °C; and (d) pore size distributions for the respective substrates.

temperature and tape pulling rate affect the morphology of the casted tape.

Fig. 1 shows the morphology features, pore size and pore size distribution of Ni–YSZ substrates with different solid loading varied from 15 vol% to 25 vol% while keeping the freezing bed temperature at −60 °C and the tape pulling rate at 48 mm min^{-1}. The acicular pores grew perpendicular to the freezing bed. There seems to be a loss of pore size and pore alignment and continuity with the increase in the solid loading of the slurry. The porosities of the Ni–YSZ substrates are 60.88%, 49.01% and 37.57% when the solids loading are 15 vol%, 20 vol% and 25 vol%, respectively. During the solidification of the slurry, the slurry changed into ice crystals and ceramic walls because the ceramic particles were rejected by the growing ice crystals. The small ice crystals can develop into large crystals in the lower solid loading slurry while the pores in freeze-tape casted samples are generated by sublimation of the ice crystals. Therefore, as shown in Fig. 1 (a), the substrate with lower solid loading has larger pores and porosity. The pore size distribution of the substrates with different solid loading can be seen in Fig. 1 (d). The average pore sizes for the substrates with solid loading of 15 vol%, 20 vol% and 25 vol% are approximately 46.64, 19.68 and 8.30 μm, respectively. The effect of solid loading on the microstructure can be attributed to the following reasons: on one hand, the bottom of the slurry in the casted tape was first frozen so that ice crystals grew very fast with many fine ice crystals resulted from the temperature gradient due to the temperature at the bottom of the slurry was lower than that at the top of slurry; on the other hand, the interaction between ceramics and ice crystals became stronger and the growth of ice crystals was hindered by the ceramic particles in the higher solid loading slurry.

Fig. 2 shows the effect of freezing bed temperature (−70 °C, −60 °C and −50 °C) on the morphology, pore size and pore size distribution of Ni–YSZ substrates while keeping the solid loading at 20 vol% and the tape pulling rate at 48 mm min^{-1}. All of the substrates show similar pore size (around 18 μm) and pore size distribution behavior due to the same solid loading. However, the difference in microstructure is still obvious. Pores grown in lower temperatures show better ordering with uniform pore size and shape. Lower freezing bed temperature can lead to slower growth rate of the ice crystals and introduce some dendritic growth of the ice crystals, as shown in Fig. 2 (a); however, this is also accompanied by a discontinuity of porosity.

Fig. 3 shows the effect of pulling rate (36, 48, 60 mm min^{-1}) on the microstructure, pore size and pore size distribution of the Ni–YSZ substrates while keeping the solid loading at 20 vol% and the freezing bed temperature at −60 °C. There are distinct differences in the morphology of the Ni–YSZ substrates although the pore size (around 18 μm) and pore size distribution characteristics are very similar. Slower tape pulling rate results in higher growth rate of the ice crystals, leading to less tortuous acicular finer pores

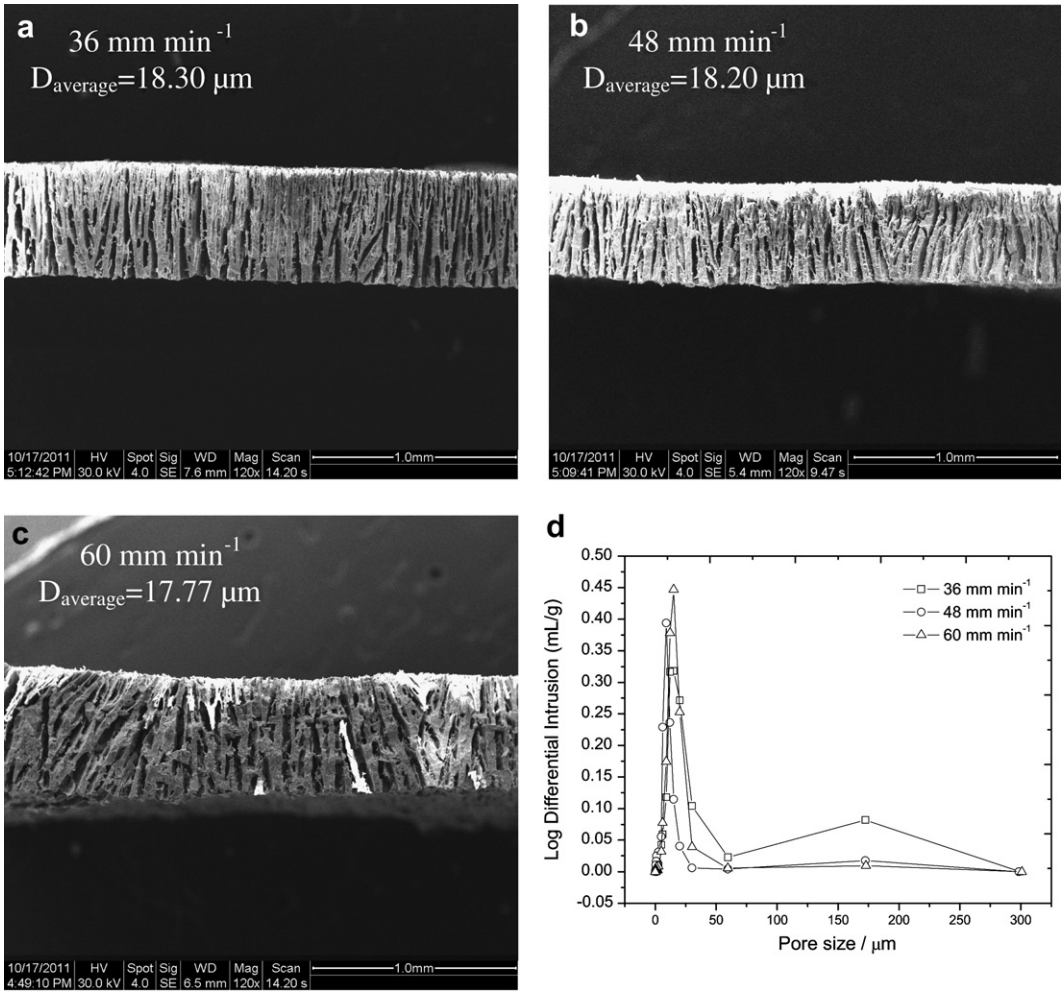

Fig. 3. Cross-section SEM images for Ni–YSZ substrate prepared from different tape pulling rate: (a) 36 mm min^{-1}; (b) 48 mm min^{-1} and (c) 60 mm min^{-1}; and (d) pore size distributions for the respective substrates.

in the low-temperature region in the substrate, which is helpful for fabrication of an interlayer or dense electrolyte film on the surface of the substrate.

This study shows that the processing parameters during the freeze-tape-casting have significant influence on the porosity and morphology of the Ni–YSZ substrates. Lower solid loading leads to larger porosity. The freezing bed temperature and pulling rate affect the growth rate of the ice crystals in the casted tape. Higher ice crystal growth rate results in straight and less tortuous finer pores. Consequently, slurry with solid loading of 20 vol%, freezing bed temperature of −70 °C and the tape pulling rate of 48 mm min^{-1} have been chosen in this work to fabricate solid oxide cells for electrochemical performance evaluation.

3.2. Electrochemical performance of button NiO–YSZ supported SOFCs

Fig. 4 shows the microstructure features of the hydrogen electrode-supported solid oxide cells and the surface view of the YSZ electrolyte. The cell has a thick NiO–YSZ gas transport layer, a thin NiO–YSZ hydrogen electrode functional layer, a thin dense YSZ layer and a thin porous LSM–YSZ layer with thickness of about 450, 15, 10 and 20 μm, respectively. The novel acicular and perpendicular pore structures seen in Fig. 4 (a) and (c) are cross-section SEM images of cell before and after the cell electrochemical performance measurement. Fig. 4 (d) shows the surface view of the YSZ electrolyte. The novel acicular and graded pores in the hydrogen electrode can be formed by the freeze-tape-casting method. The dense YSZ electrolyte is well adhered to the electrodes. The presence of acicular pores in the hydrogen electrode substrate will facilitate mass transport of the reactants to the TPB in the functional layer, thus accelerating the electrochemical reactions in the electrode.

Fig. 5 (a) shows the cell voltage, current and power output curves of cells under the SOFC mode at different temperatures. Fig. 5 (b) compares the cell power output of cells prepared by either dry-pressing or freeze-tape-casting method. As shown in Fig. 5 (a), the cell peak power densities are 0.60, 0.95 and 1.28 W cm^{-2} at 700, 750 and 800 °C, respectively, almost doubled the cell output values previously reported at similar testing conditions with similar cell materials [15]. Under similar testing conditions, the cell power output for cells fabricated by freeze-tape-casting method is much higher than that of cells fabricated by dry-pressing method (see Fig. 5 (b)). The cell performance is even higher than the previous study of the hydrogen electrode with ceria oxide modification [16], further demonstrating the advantage of the novel acicular pore structure in the hydrogen electrode substrate.

Fig. 6 (a) shows the impedance spectra of cells measured at different temperatures under open circuit conditions. The cell ohmic resistance (R_Ω), corresponding to the high frequency intercept of the impedance spectra with the real axis in the Nyquist plot, is 0.14, 0.10 and 0.08 Ω cm^2 at 700, 750 and 800 °C, respectively. The cell polarization resistance (R_p), determined from the difference between the high and low frequency intercepts of the impedance spectra with the real axis, is about 0.80, 0.32 and 0.17 Ω cm^2 at 700, 750 and 800 °C, respectively. As shown in Fig. 6 (b) and (c), in

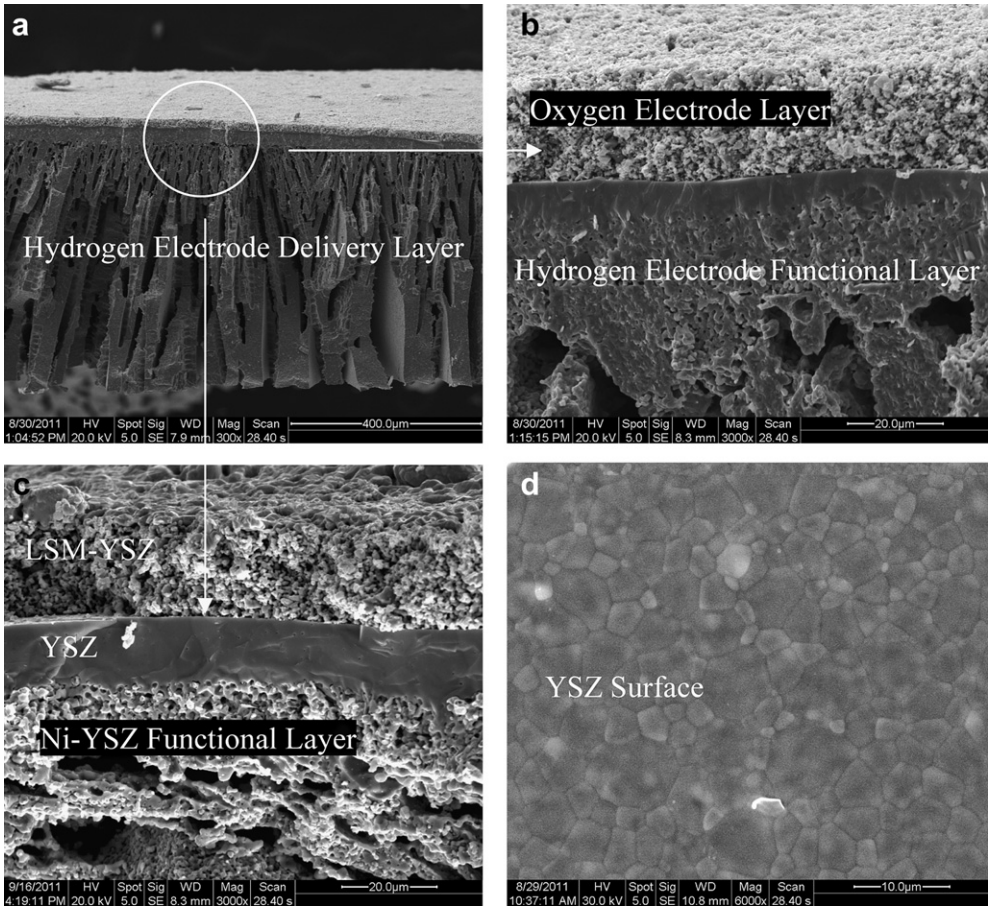

Fig. 4. SEM images of: (a) and (b) cross section view of the cell before testing; (c) cross section view of the cell after electrochemical performance measurement and (d) surface of electrolyte YSZ before the cell electrochemical performance measurement.

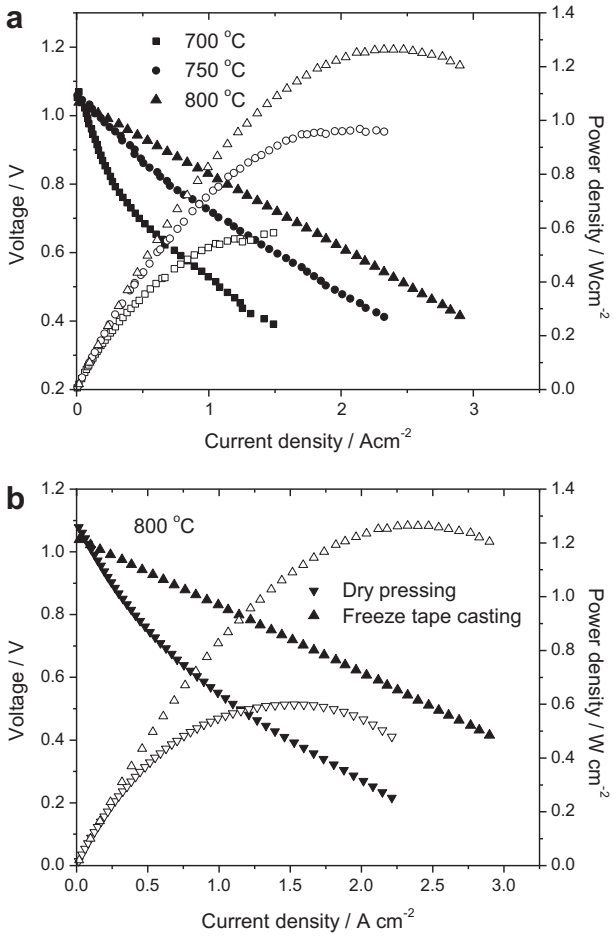

Fig. 5. (a) IV and IP curves of cell measured at different temperatures using hydrogen as fuel and ambient air as oxidant; (b) Comparison of IV and IP curves of cells prepared by either dry-pressing or freeze-tape-casting method measured at 800 °C.

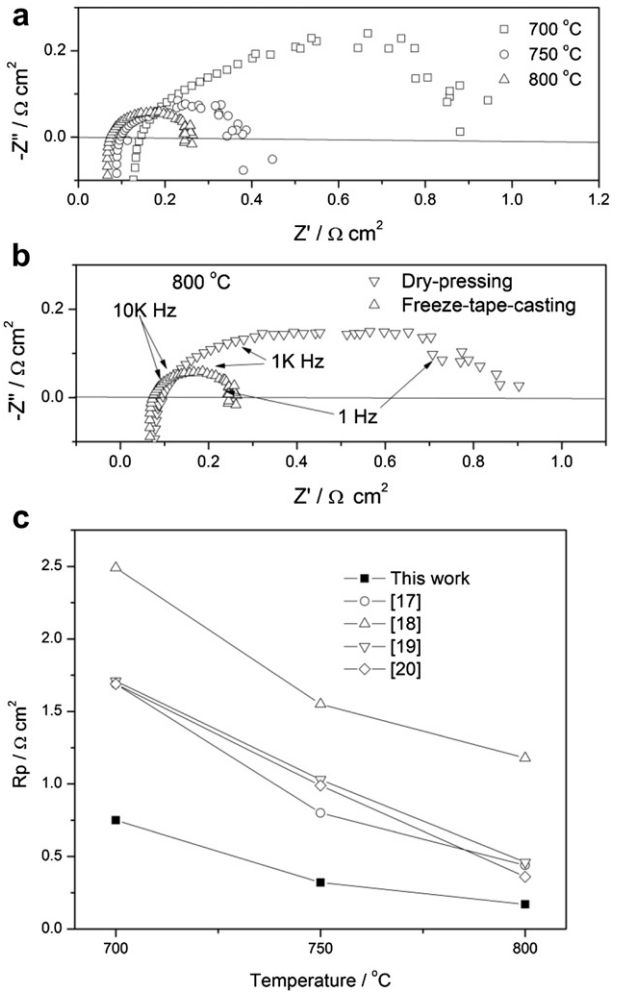

Fig. 6. (a) Impedance spectra of cells tested at different temperature under open circuit conditions, (b) Comparison of impedance spectra of cells fabricated by either dry-pressing or freeze-tape-casting method measured at 800 °C and (c) Comparison of the cell R_p with other publications.

comparison to the interfacial resistance of the cells fabricated by freeze-tape-casting, dry-pressing and other publications [17–20], the total cell electrode polarization resistances in this study are much lower. The cell electrode polarization resistance comes from the resistance of the gas diffusion and gas conversion, i.e., gas diffusion and electrochemical conversion in both the anode and the cathode. Since the materials for both the anode and the cathode are almost identical, and the fabrication method, the thickness and microstructure of the cathode are similar in all the different studies, the decrease in the cell polarization resistance could be attributed to the enhancement of the anode performance, probably due to the decreased hydrogen/water diffusion limit. The gas diffusion resistance through the anode can be estimated by the following equation [7,21]:

$$R_{\text{Diffusion(anode)}} = \left(\frac{RT}{2F}\right)^2 l_a \frac{1}{D_{H_2O,H_2}} \frac{\tau_a}{\rho_a} \left(\frac{1}{p_{H_2}} + \frac{1}{p_{H_2O}}\right) \times \left(1.0133 \times 10^5 \frac{\text{Pa}}{\text{atm}}\right)^{-1} \quad (1)$$

where $R_{\text{Diffusion(anode)}}$ is the gas diffusion resistance in the anode, R is the universal gas constant, T is the absolute temperature, F is the Faraday's constant, l_a is the anode thickness, $D_{H_2O,\,H_2}$ is the binary diffusion coefficient for a mixture of H_2O and H_2, τ_a is the tortuosity factor of the hydrogen electrode, and ρ_a is the volume fraction porosity of the anode, p_{H_2} and p_{H_2O} are the partial pressure of hydrogen and water vapor in the hydrogen electrode. The tortuosity factor for the anode substrate by freeze-tape-casting process is about 2, as obtained from mercury intrusion method, while the value for the anode substrate made from other traditional methods is typically between two to six with values even as high as ten [22]. Therefore, the gas diffusion resistance from the anode fabricated by freeze-tape-casting process is much lower, thus leading to enhanced cell performance.

Fig. 7 shows the cell performance under both the fuel cell and electrolysis modes. H_2 with a flow rate of 40 sccm was used as the carrier gas and the absolute humidity (AH) was controlled at 30% in the hydrogen electrode while the oxygen electrode was exposed to ambient air. The details about the SOEC setup and measurement have been given in our previous publication [14]. The current of the cell was obtained by decreasing the cell voltage from 1.6 to 0.2 V with a 30 mV s^{-1} sweeping rate. As shown in Fig. 7, the negative current densities indicate electrolysis mode, and the cell voltage at zero current densities refers to open circuit voltage. It can be seen that the increase in the cell operating temperature can lead to improvement of the cell current density. At 30% AH, a cell current density value of 2.3 A cm^{-2} was observed at 800 °C with an applied cell potential of 1.6 V, which is better than our previous results

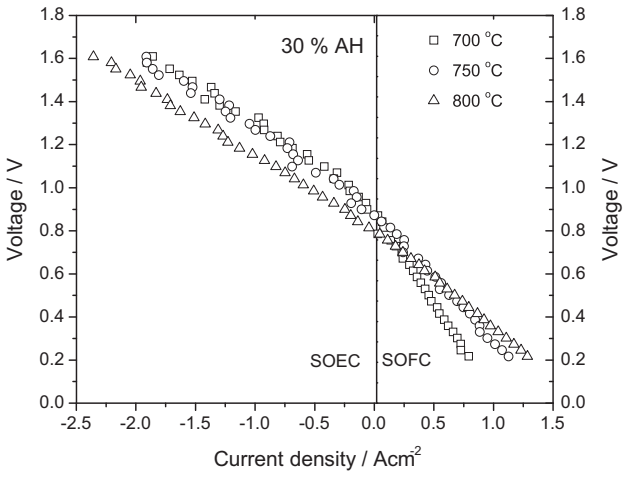

Fig. 7. Voltage–current density of cell recorded as a function of different operating temperature at 30 vol% absolute humidity in the hydrogen electrode.

under similar testing conditions under the electrolysis mode [14,23]. It is believed that the acicular pores in the hydrogen electrode help facilitate diffusion of H_2O and H_2 molecules during the electrolysis process. In addition, the cell voltage varies linearly with the cell current density ($d^2V/di^2 = 0$), different from our previously convex-up curve at higher current density region in the electrolysis mode ($[d^2V/di^2>0]$) [23], indicating that gas diffusion resistance becomes much smaller in this study. Therefore, it can be concluded that the enhancement of the cell performance under the electrolysis mode can be attributed to the acicularly porous hydrogen electrode microstructure, which facilitates gas diffusion.

4. Conclusions

A novel functionally graded and acicular hydrogen electrode supported solid oxide cell has been prepared and evaluated for both SOFCs and SOECs. The novel hydrogen electrode structure has shown significant enhancement on the cell electrochemical performance using the conventional cell materials. The cell demonstrates a maximum power density of 1.28 W cm^{-2} and a polarization resistance of 0.166 Ω cm^2 at 800 °C with 3% H_2O humidified H_2 as fuel and ambient air as oxidant in the fuel cell mode. A current density of 2.3 A cm^{-2} can be obtained at 30 vol% absolute humidity at 800 °C with an applied voltage of 1.6 V in the electrolysis mode. These results indicate that the novel functionally graded and acicular hydrogen electrode significantly facilitates gas diffusion, thus decreasing the concentration polarization resistance and enhancing the cell performance.

Acknowledgement

We gratefully acknowledge the financial support from NASA EPSCoR (Award Number NNX10AN33A), National Science Foundation (Award Number CBET 0967166), and the SC Space Grant Consortium.

References

[1] S.C. Singhal, Solid State Ionics 152–153 (2002) 405–410.
[2] C. Jin, C. Yang, F. Chen, J. Membrane. Sci. 363 (2010) 250–255.
[3] C. Yang, C. Jin, F. Chen, Electrochem. Commun. 12 (2010) 657–660.
[4] T. Werber, Solid State Ionics 42 (1990) 205–211.
[5] T. Suzuki, Z. Hasan, Y. Funahashi, T. Yamaguchi, Y. Fujishiro, M. Awano, Science 325 (2009) 852–855.
[6] M.H.D. Othman, N. Droushiotis, Z. Wu, G. Kelsall, K. Li, Adv. Mater. 23 (2011) 2480–2483.
[7] J.-W. Kim, A.V. Virkar, K.-Z. Fung, K. Mehta, S.C. Singhal, J. Electrochem. Soc. 146 (1999) 69–78.
[8] S.W. Sofie, J. Am. Ceram. Soc. 90 (2007) 2024–2031.
[9] T.L. Cable, S.W. Sofie, J. Power Sources 174 (2007) 221–227.
[10] P. Gannon, S. Sofie, M. Deibert, R. Smith, V. Gorokhovsky, J. Appl. Electrochem. 39 (2009) 497–502.
[11] M.D. Gross, J.M. Vohs, R.J. Gorte, Electrochem. Solid State Lett. 10 (2007) B65–B69.
[12] Z. Wang, N. Zhang, J. Qiao, K. Sun, P. Xu, Electrochem. Commun. 11 (2009) 1120–1123.
[13] T.L. Cable, J.A. Setlock, S.C. Farmer, A.J. Eckel, Int. J. Appl. Ceram. Technol. 8 (2011) 1–12.
[14] C.H. Yang, A. Coffin, F.L. Chen, Int. J. Hydrogen Energy 35 (2010) 3221–3226.
[15] Y.J. Leng, S.H. Chan, K.A. Khor, S.P. Jiang, Int. J. Hydrogen Energy 29 (2004) 1025–1033.
[16] W. Zhu, C. Xia, J. Fan, R. Peng, G. Meng, J. Power Sources 160 (2006) 897–902.
[17] L. Zhang, S.P. Jiang, W. Wang, Y. Zhang, J. Power Sources 170 (2007) 55–60.
[18] X. Xin, Z. Lü, X. Huang, X. Sha, Y. Zhang, W. Su, J. Power Sources 159 (2006) 1158–1161.
[19] L. Zhang, J. Gao, M. Liu, C. Xia, J. Alloy. Compd. 482 (2009) 168–172.
[20] Y. Chen, F. Chen, W. Wang, D. Ding, J. Gao, J. Power Sources 196 (2011) 4987–4991.
[21] A.V. Virkar, J. Chen, C.W. Tanner, J.-W. Kim, Solid State Ionics 131 (2000) 189–198.
[22] E.L. Cussler, Diffusion: Mass Transfer in Fluid Systems, Cambridge University Press, Cambridge, 1995.
[23] C. Yang, C. Jin, A. Coffin, F. Chen, Int. J. Hydrogen Energy 35 (2010) 5187–5193.